Crystallography of graphite spheroids in cast iron

Koenraad Theuwissen, Lydia Laffont-Dantras, Muriel Véron, Jacques Lacaze

Crystallography of graphite spheroids in cast iron

K. Theuwissen[1]*, L. Laffont[1], M. Véron[2] and J. Lacaze[1]

To further understand graphite growth mechanisms in cast irons, this study focuses on the crystal structure of a graphite spheroid in the vicinity of its nucleus. A sample of a graphite spheroid from a commercial cast iron was characterised using transmission electron microscopy. The chemical composition of the nucleating particle was studied at the local scale. Crystal orientation maps of the graphite spheroid revealed misorientations and twist boundaries. High resolution lattice fringe images showed that the basal planes of graphite were wavy and distorted close to the nucleus and very straight further away from it. These techniques were complementary and provided new insights on spheroidal graphite nucleation and growth.

Keywords: Graphite growth, Heterogeneous nucleation, Crystal orientation, Transmission electron microscopy

Introduction

Since the discovery of the graphite spheroidisation treatment in cast irons, much research has been carried out to understand the development of spheroidal graphite precipitates. Various spherulitic growth models have been proposed,[1–6] but the formation of this peculiar morphology remains unclear. The first step to understand this phenomenon is nucleation, and the general agreement is that graphite nucleates heterogeneously on foreign particles issued from the inoculation treatment. Several studies have focused on the nature of the nuclei: non-metallic inclusions have been found at the centre of graphite spheroids and have thus been considered as nucleation sites for graphite. The nucleation potential of these inclusions has been related to mismatch between their lattice parameters and that of graphite. The main types of nuclei quoted in the literature are salt-like carbides such as CaC_2[7,8] and various combinations of sulphides, oxides and silicates.[9–13] It has been stated that the same type of exogenous nuclei can produce both flake and spheroidal graphite, suggesting that the growth process determines the morphology of the graphite precipitates.[10,12,14,15] This paper illustrates the growth of a graphite spheroid from a nucleating particle as imaged by transmission electron microscopy.

Experimental

The investigated spheroidal graphite cast iron is a standard ferritic alloy used in previous work[16] and containing mainly 3.64 wt-%C and 2.05 wt-%Si (Table 1). Nodularising treatment was made by the sandwich method using a 50 kg capacity ladle, at the bottom of which was placed 1.3 wt-% of a FeSiMg alloy (42–44 wt-%Si, 5–6 wt-%Mg, 0.9–1.0 wt-%Ca, 0.4–0.5 wt-%Al, 0.9–1.1 wt-%RE). The alloy was cast in chemically bonded sand moulds that contained standard keel blocks as described elsewhere.[17] Inoculation was carried out by adding ~0.15 wt-% of a commercial inoculant (68.1 wt-%Si, 0.89 wt-%Al, 1.65 wt-%Ca, 0.45 wt-%Bi, 0.38 wt-%Ba, 0.37 wt-%RE) into the cavity of the mould. A sample of this iron was ground and mirror polished with a 0.05 μm alumina suspension for metallographic examination. The graphite precipitates were of high nodularity; their surface density was evaluated at 400 mm^{-2} and their mean diameter at 19 μm.

A transmission electron microscopy TEM specimen was extracted from this sample. In order to obtain a diametrical section of the spheroid, a JEOL JIB-4600F focused ion beam (FIB) scanning electron microscope (SEM) a was used. Figure 1 shows the area for extraction of the specimen using the FIB lift-out technique. TEM investigation was carried out using a JEOL JEM-2100F transmission electron microscope at the Temscan service of Paul Sabatier University, operated at 200 kV. This microscope was equipped with a Bruker Quantax silicon drift detector, which enabled-energy dispersive X-ray analysis (EDX).

Automated crystal orientation mapping (ACOM) was carried out in a JEOL 3010 TEM at the SIMaP laboratory, operated at 300 kV, equipped with a DigiStar external source with step size of 17 nm. This technique enables investigation of crystal orientations at high spatial resolution based on electron diffraction patterns.[18,19] Moreover, difficulties in determining crystal orientations of carbon-based materials found with other techniques such as EBSD can be overcome using ACOM.

Results and discussion

Figure 2 is a photomontage of bright field images showing a complete view of the sample. The central part of the sample shows a different contrast than that of the rest of the sample, which is shown enlarged in Fig. 3. These figures show that conical sectors radiate outwards from this

[1]CIRIMAT, Université de Toulouse, ENSIACET, CS 44362, 31030 Toulouse cedex 4, France
[2]SIMAP Laboratory, CNRS-Grenoble INP, BP 46, 101 rue de la Physique, 38402 Saint Martin d'Hères, France

*Corresponding author, email: koenraad.theuwissen@ocas.be

DOI 10.1179/1743133615Y.0000000028

Table 1 Sample composition

Element	C	Si	Mn	P	S	Mg	Cu	Fe
wt-%	3.64	2.05	0.11	0.033	0.015	0.037	0.04	Bal.

central area, strongly suggesting that the central part of the specimen corresponds to a nucleating particle.

The bright field image of the central area (Fig. 3) shows the clear difference in contrast between the nucleus and the surrounding graphite, as well as contrast differences between several parts of the nucleus. Energy dispersive X-ray analyses were performed at various locations in the central area and showed that the chemical composition of the nucleus is not homogeneous. It is relevant to note that sulphur content was not evaluated in this study because the sample was mounted on a molybdenum holder, whose Lα1 X-ray line produces a severe overlap with the Kα1 of sulphur.

The results are presented in Table 2, where it is seen that the inner part of the nucleus contains mainly Mg and Ca (the reported C values may not be significant except for the measurement #9 in graphite). Discrete particles at the periphery of the nucleus may be sorted as either Fe rich or Mg rich. These latter particles do contain Bi, La and Ca as well. Only in one occasion was oxygen detected at a significant level (particle #1), but it is not possible to ascertain that graphite nucleated at that location, i.e. to confirm that graphite nuclei are duplex sulphide oxide particles.[10] Given the shape of the observed particles, it is unlikely that a continuous oxide shell surrounds the core of the present nucleus as has been reported in the case of nuclei with duplex compositional structures.

Spectra were also taken on graphite in the vicinity of the nucleus, as seen in point 9 of Fig. 3. Elements from the nucleus were not detected at any significant level within graphite, suggesting that the particle serves solely as a nucleant.

The crystallographic features of graphite were investigated by means of selected area electron diffraction patterns, which were taken at different locations around the nucleus using an aperture with a 250 nm diameter as shown in Fig. 4. These patterns show several (0002) spots or diffraction arcs revealing different *c* axes orientations in the selected areas and their relative misorientations can be measured directly on the diffraction patterns. This information was used to identify several growth sectors according to the orientation of the *c* axes of graphite. For clarity, the apparent boundaries between sectors were drawn in the bright field image of Fig. 4, and only the (0002) spots were labelled in the corresponding diffraction patterns.

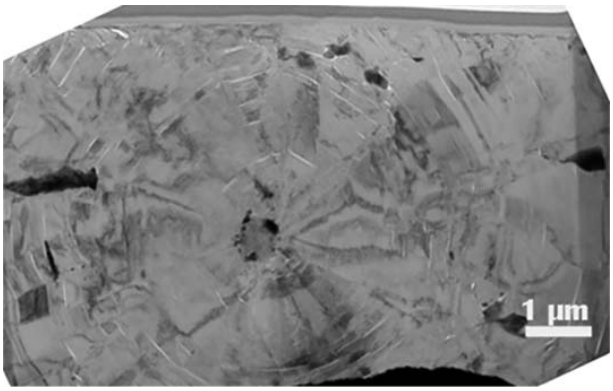

2 Bright field TEM images showing overview of specimen

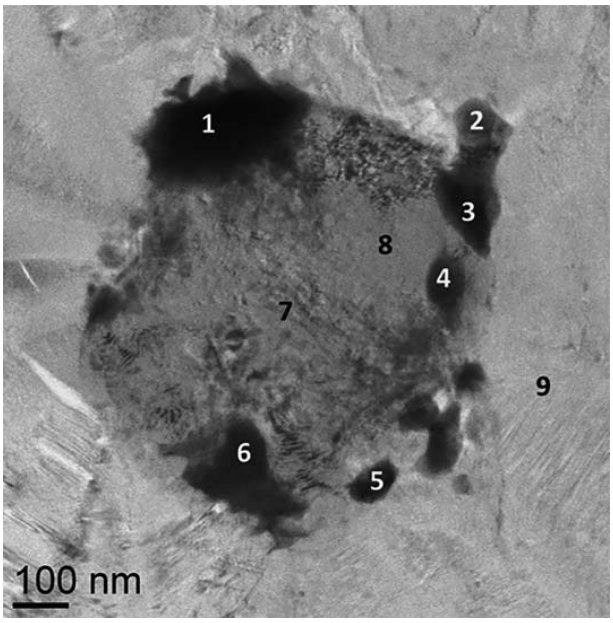

3 Bright field TEM image of nucleus

In order to have a general view of the orientations of graphite, ACOM measurements were carried out over an area of ~4 μm around the nucleus. Figure 5 shows orientation maps projected along two different axes. The overall conical shape of the orientation domains is seen, and misorientations are revealed by the colour changes. These can be considered as growth defects (tilts or twists as defined in earlier studies of graphite crystals[20]).

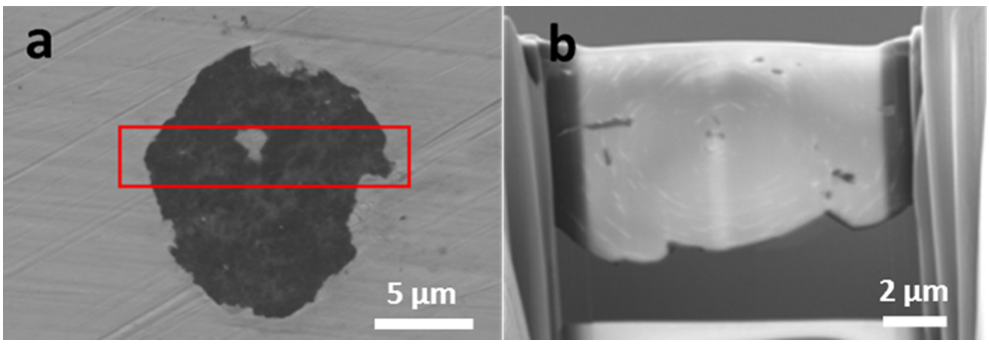

1 Images (SEM) illustrating sample preparation using FIB lift out technique

Table 2 Corresponding to the areas numbered in figure 3 EDX analyses*/at- %

	1	2	3	4	5	6	7	8	9
Fe	5.9	85.3	25.4	0.7	77.7	1.3	0.2	0.2	N.D.
Si	5.2	5.9	1.3	0.3	3.8	N.D.	0.5	0.8	N.D.
Mg	32.8	0.4	1.1	65.8	14.3	54.5	48.6	61.1	N.D.
La	7.6	8.4	0.5	5.2	1.5	10.6	2.7	N.D.	N.D.
Bi	7.9	N.D.	N.D.	11.7	N.D.	21.2	N.D.	N.D.	N.D.
O	33.6	N.D.	1.6	N.D.	N.D.	0.1	1.5	0.5	0.1
Ca	7.2	N.D.	0.1	16.3	2.7	12.3	11.1	20.5	N.D.
C	N.D.	N.D.	70.	N.D.	N.D.	N.D.	35.4	16.9	99.9

*N.D.: no-detected.

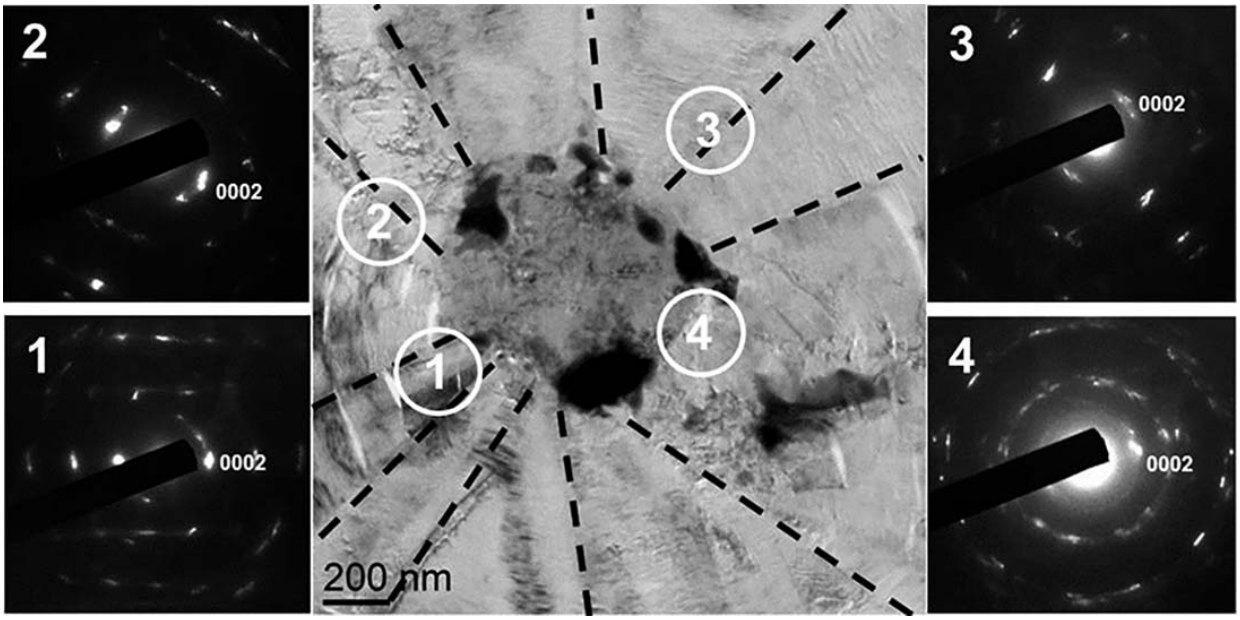

4 Identification of growth sectors using selected area electron diffraction

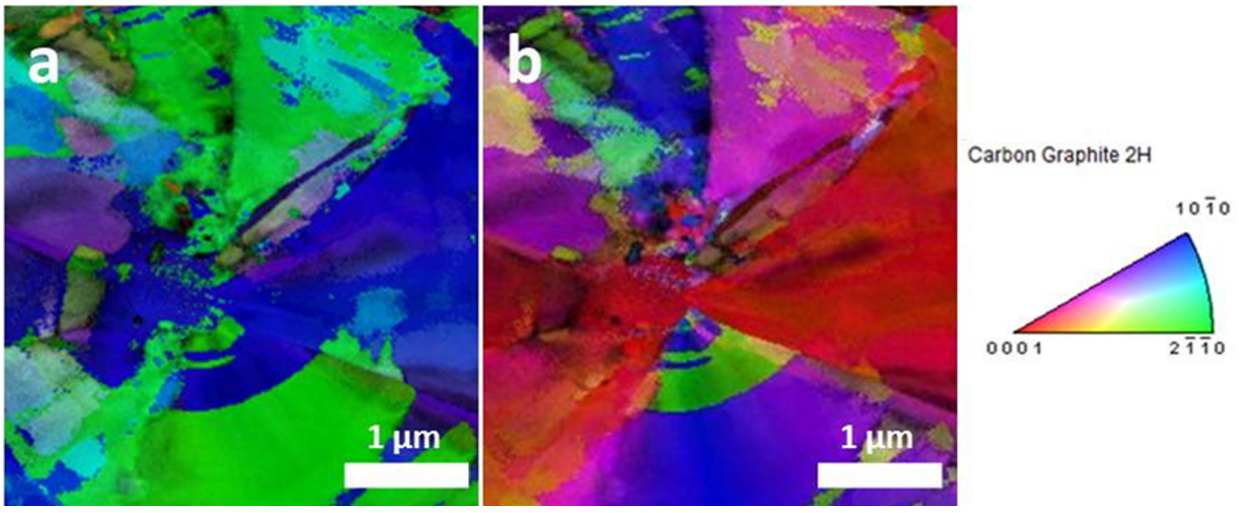

5 Crystal orientation maps of graphite in central part of specimen. Projections along sample's normal direction and *a* along horizontal sample's length *b*

Measurements proved that the misorientations values around the nucleus are relatively small, mainly 5° to 10° and 11° to 13°. In some cases, higher misorientation values were observed within sectors: the changes from green to blue in Fig. 5*a* correspond to rotations of 27.5° and 25.8° around the *c* axis of graphite. The rotation angles close to 27° reported here correspond to low energy stacking faults in graphite as reported experimentally and predicted by the coincidence site lattice theory[3,21–23] and could provide sites for atom

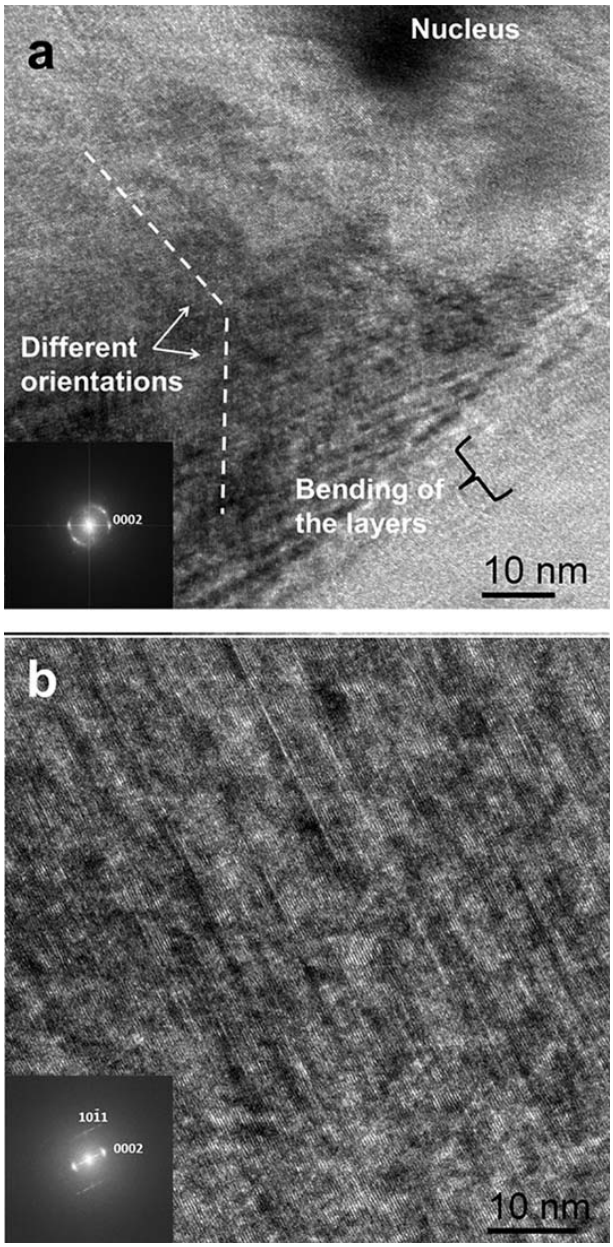

6 Lattice fringe images and corresponding FFT (inserts) taken *a* close in nucleus and *b* further away in sector

attachment on prismatic planes as suggested for the growth of graphite flakes.[24]

The structure of graphite close to the nucleus was further studied using 0002 lattice fringe imaging mode for direct visualisation of the graphene layers. Micrographs such as the one presented in Fig. 6*a* show that graphene layers are often bent and curved in the vicinity of the nucleus leading to orientation changes as shown in the corresponding fast Fourier transform (FFT) of the image in the insert. This could be explained by the fact that such rippling occurs at the interface between neighbouring sectors, as reported elsewhere.[25] As several sectors grow from the nucleus (Fig. 4) their junction will inevitably lead to defects and consequently misorientations. The image in Fig. 6*b* was taken at about 1.5 μm from the nucleus, and shows relatively straight fringes with few defects and its FFT (insert) shows accordingly one main orientation.

Conclusions

A thin foil specimen was extracted from a graphite spheroid and was studied by means of transmission electron microscopy. The presence of a foreign particle at the centre of the specimen was regarded as evidence that this was a diametrical section of the spheroid, well suited for a nucleation and growth study. The chemical composition of the nucleus was not homogeneous: the central part contains mainly Ca and Mg, whereas discrete particles rich in either Fe or Mg appeared at the outer surface of the nucleus.

Crystal orientation maps revealed the extent of sectoral growth from the nucleating particle. Misorientations were observed, and the identification of rotation boundaries at several locations in the sample seems closely related to the mechanism of spheroidal growth as they are much less observed in lamellar growth.[25]

The visualisation of graphene layers using high resolution TEM showed their extensive deformation in the vicinity of the nucleating particle.

Studying the structure of graphite in the vicinity of the nucleus in other types of precipitates would be of interest to understand how the first stages of growth lead to the development of different graphite morphologies, but the main difficulty lies in locating the nucleus to produce appropriate TEM specimens.

Acknowledgements

The authors acknowledge T. Suzuki and H. Matsushima at JEOL-Japan for the FIB sample preparation.

References

1. M. Hillert and Y. Lindblom: 'The growth of nodular graphite', *J. Iron. Steel Res. Inst.*, 1954, **148**, 388–391.
2. J. P. Sadocha and J. E. Gruzleski: 'The mechanism of graphite spheroid formation in pure Fe-C-Si alloys', *Proc. Metal. Cast Iron*, 1974, 442–459.
3. D. D. Double and A. Hellawell: 'Cone-helix growth forms of graphite', *Acta Metall.*, 1974, **22**, 481–487.
4. B. Miao, D. O. Northwood, W. Bian, K. Fang and M. H. Fan: 'Structure and growth of platelets in graphite spherulites in cast iron', *Journal of Materials Science*, 1994, **29**, 255–261.
5. G. Faivre: 'On the mechanisms of spherulitic growth in polymer and iron melts', *Adv. Mater. Res.*, 1997, **4-5**, 17–30.
6. D. D. Double and A. Hellawell: 'The nucleation and growth of graphite. The modification of cast iron', *Acta Metall. Mater.*, 1995, **43**, 2435–2442.
7. B. Lux: 'On the theory of nodular graphite formation in cast iron – Part I: experimental observations of nodular graphite formation during the solidification of cast iron melts', *Giessereifoschung in English*, 1970, **22**, 65–81.
8. B. Lux: 'On the theory of nodular graphite formation in cast iron – Part II: theoretical interpretation of the experimental observations', *Giessereifoschung in English*, 1970, **22**, 158–177.
9. M. H. Jacobs, T. J. Law, D. A. Meldford and M. J. Stowell: 'Basic processes controlling the nucleation of graphite nodules in chill cast irons', *Met. Technol.*, 1974, **1**, 490–500.
10. M. H. Jacobs, T. J. Law, D. A. Meldford and M. J. Stowell: 'Identification of heterogenous nuclei for graphite spheroids in chill-cast iron', *Met. Technol.*, 1976, **3**, 98–108.
11. M. J. Lalich and J. R. Hitchings: 'Characterization of inclusions as nuclei for spheroidal graphite in ductile cast irons', *AFS Trans.*, 1976, **84**, 653–664.
12. B. Francis: 'Heterogeneous nuclei and graphite chemistry in flake and nodular cast irons', *Metall. Mater. Trans. A, 10A*, 1979, 21–31.
13. T. Skaland, O. Grong and T. Grong: 'A model for the graphite formation in ductile cast iron: Part I. Inoculation mechanisms', *Metall. Trans. A*, 1993, **24A**, 2321–2345.
14. G. Ostberg: 'Perspectives on research on the formation of nodular graphite in cast iron', *Mater. Des.*, 2006, **27**, 1007–1015.

15. A. Velichko: 'Quantitative 3D characterization of graphite morphologies in cast iron using FIB microstructure tomography', 'PhD thesis, Universität des Saarlandes, Saarbrücken, Germany',; 2008.
16. N. Valle, K. Theuwissen, J. Sertucha and J. Lacaze: 'Effect of various dopant elements on primary graphite growth', *IOP Conf. Ser. Mater. Sci. Eng.*, 2012, **27**, 012026.
17. I. Asenjo, J. Lacaze, P. Larrañaga, S. Mendez, J. Sertucha and R. Suarez: 'Microstructure investigation of small-section nodular iron castings with chunky graphite', *Key Eng. Mater.*, 2011, **457**, 52–57.
18. E. F. Rauch and M. Veron: 'Coupled microstructural observations and local texture measurements with an automated crystallographic orientation mapping tool attached to a tem', *J. Mater. Sci. Eng. Technol.*, 2005, **36**, 552–556.
19. E. F. Rauch, M. Veron, J. Portillo, D. Bultreys, Y. Maniette and S. Nicolopoulos: 'Automatic crystal orientation and phase mapping in TEM by precession diffraction', *Microsc. Microanal.*, 2008, **22**, S5–S8.
20. S. B. Austerman, S. M. Myron and J. W. Wagner: 'Growth and characterization of graphite single crystals', *Carbon*, 1967, **5**, 549–557.
21. I. Minkoff and S. Myron: 'Rotation boundaries and crystal growth in the hexagonal system', *Philos. Mag.*, 1968, **19**, 379–387.
22. D. D. Double and A. Hellawell: 'Defects in eutectic flake graphite', *Acta Metall.*, 1971, **19**, 1303–1306.
23. A. Roviglione and J. D. Hermida: 'X-ray diffraction characterization of flake and compacted graphite in cast iron', *Mater. Charact.*, 1994, **32**, 127–137.
24. I. Minkoff and B. Lux: 'Graphite growth from the melt', *Proc. Metall. Cast Iron*, 1974, 473–491.
25. K. Theuwissen: 'Etude de l'influence des impuretés et des éléments à l'état de traces sur les mécanismes de croissance du graphite dans les fontes', 'PhD thesis, Université de Toulouse, Toulouse, France'; 2013. http://ethesis.inp-toulouse.fr/archive/00002393/.